Applied Catalysis B: Environmental 193 (2016) 234–239

Contents lists available at ScienceDirect

Applied Catalysis B: Environmental

journal homepage: www.elsevier.com/locate/apcatb

Low-temperature NO-adsorption properties of manganese oxide octahedral molecular sieves with different potassium content

Tsuyoshi Hamaguchi[a,*], Toshiyuki Tanaka[a], Naoko Takahashi[a], Yoshihisa Tsukamoto[b], Nobuyuki Takagi[b], Hirofumi Shinjoh[a]

[a] Toyota Central Research and Development Labs., Inc., Nagakute, Aichi 480-1192, Japan
[b] Toyota Motor Corporations, Toyota, Aichi 471-8572, Japan

ARTICLE INFO

Article history:
Received 9 December 2015
Received in revised form 11 April 2016
Accepted 12 April 2016
Available online 14 April 2016

Keywords:
Nitric oxide
Adsorbent
Manganese oxide octahedral molecular sieves

ABSTRACT

In this study, we synthesized hollandite-type manganese oxide octahedral molecular sieves (OMS) with different potassium content ($K_xMn_8O_{16}$; K-OMS-2). Owing to crystal growth, the specific surface area of K-OMS-2 decreased with an increase in the K concentration for $x > 1.5$. The K-OMS-2 samples with $x < 1.5$ exhibited NO adsorption at low temperatures because of an oxidation reaction of NO. The amount of adsorbed NO depended on the oxidation activity of K-OMS-2 instead of the specific surface area (i.e., the number of NO adsorption sites). The amount of NO that was adsorbed at 323 K was correlated to the increase in the amount of oxygen released from K-OMS-2. It is assumed that the thermally unstable oxygen sites acted as oxidation sites for NO at low temperatures and thus increased the amount of adsorbed NO.

1. Introduction

The development of high-performance catalytic systems is necessary for meeting stricter emission regulations in the future. It is difficult to remove NO_x from the exhaust gases emitted from lean-burn and diesel engines at temperatures below 473 K using NO_x-storage reduction or selective catalytic reduction systems, which operate under excess-oxygen conditions [1]. In order to address this issue, NO_x adsorbents such as $BaSnO_3$ [2], MnCe oxide [3], MnZr oxide [4], Ag/Al_2O_3 [5], and $Ag/Ti/Al_2O_3$ [6], which exhibit excellent NO adsorption activities at low temperatures, have been studied. However, CO, CO_2, H_2O, and the hydrocarbons present in exhaust gases decrease the adsorption activity of these materials at temperatures below 373 K. CO_2 and H_2O are present in the exhaust gases in high percentages, and they retard the physical adsorption of NO. In order to adsorb NO in exhaust gases at temperatures below 373 K, the adsorbent has to oxidize NO to NO_x. Therefore, it is critical for low-temperature NO adsorbents to exhibit high oxidation activity with respect to NO_x.

Recently, researchers have focused on octahedral molecular sieves (OMS) made of hollandite-type manganese oxide (OMS-2: $A_xMn_8O_{16}$, $0 < x < 2$) because of their unique structure. In these materials, a 2×2 edge and the corner-shared MnO_6 octahedron forms a one-dimensional microporous tunnel structure with a pore size of ~0.46 nm. Moreover, in this tunnel, K^+, NH_4^+, Na^+, Ba^{2+}, and H^+ ions generally occupy the tunnel sites (A sites) [7–10]. Previous studies suggested that manganese has mixed valency (Mn^{4+}, Mn^{3+}, and Mn^{2+}) in this framework [11]. A few studies have also been published on OMS-2 as a catalyst for the selective catalytic reduction of NH_3 [12]; as a battery material [13]; a catalyst for the oxidation of CO, volatile organic compounds, alcohol, and other hydrocarbons [14–21]; and as a gas absorbent [22]. Gandhe et al. suggested that the ready availability of lattice oxygen from OMS-2 facilitates the oxidation process [23].

In order to alter the catalytic, thermal, and structural properties of OMS-2, a few alkaline metals and hydrogen have been successfully incorporated into OMS-2 as metal dopants. Kumar et al. reported that the proton-exchanged OMS-2 (H-K-OMS-2) exhibited higher activity than K-OMS-2 (in which K occupies the A site) in the condensation of phenyl hydroxylamine with aniline to produce 2-aminodiphenylamine [10]. Yin et al. reported that the thermal stability of ion-exchanged OMS-2 was slightly lower than that of undoped OMS-2 [9]. Thus, variations in the type of ions occupying

Abbreviations: AOS, average oxidation number; DRIFTS, diffuse reflectance infrared Fourier-transform spectroscopy; FTIR, Fourier-transform infrared; RT, room temperature; SSA, specific surface area; TEM, transmission electron microscopy; TG/DTA, thermogravimetry/differential thermal analysis; XAFS, X-ray absorption fine structure; XPS, X-Ray photoelectron spectroscopy; XRD, X-ray diffraction.

* Corresponding author.
E-mail address: e1394@mosk.tytlabs.co.jp (T. Hamaguchi).

http://dx.doi.org/10.1016/j.apcatb.2016.04.023
0926-3373/

the A sites lead to changes in the physical, chemical, and catalytic properties of OMS-2.

Based on the above developments, we attempted to develop high-performance catalysts like K-OMS-2 as low-temperature NO-adsorbing materials. In order to understand the NO-adsorption activity in real exhaust gases, the adsorption of NO on K-OMS-2 was tested in a flow reactor in the presence of interfering gases such as CO_2 and H_2O. Under such conditions, the NO-oxidation activity plays a bigger role than the number of adsorption site in determining the NO-adsorption performance. Since K-OMS-2 is a well-known high-performance oxidation catalyst, we expect it to be a suitable NO-adsorbing material at low temperature. Herein, we report the results of our investigation and discuss the NO_x-adsorption mechanism based on characterizations of K-OMS-2.

2. Experimental

2.1. Material synthesis

K-OMS-2 was prepared by a solvent-free method described in a previous report [24]. $KMnO_4$ and $Mn(Ac)_2{\cdot}4H_2O$ powders were mixed together and ground for 30 min. This powder mixture was then placed on a glass plate and aged at 353 K for 4 h. The black product was washed with deionized water several times (Table 1) to remove any ions that may have remained in the product; it was then dried overnight in air at 383 K. The washed and dried product was calcined at 773 K. To control the occupancy rate of the K sites, we varied the $KMnO_4$/Mn(Ac) mixing ratio and the number of times we washed the black product, as shown in Table 1. A few of the samples were washed with 0.01 mol/L HNO_3 or 25 wt% NH_3 to remove K from the K-OMS-2 samples.

2.2. Characterization methods

The synthesized samples were characterized by the following methods. The morphology of the samples was observed by transmission electron microscopy (TEM; JEM-2010FEF, JEOL, Japan). The crystal structure of the samples was characterized by X-ray diffraction (XRD; RINT-TTR, Rigaku, Japan) using Cu Kα radiation (λ = 0.15418 nm) at 40 kV and 30 mA. The XRD patterns were obtained in the continuous scanning mode at a 2θ scanning speed of 5°/min. The crystallite sizes of K-OMS-2 were calculated from the (211) diffraction lines using Scherrer's equation. Thermograms were obtained with a thermogravimetric differential thermal analyzer (TG-DTA; Thermo Plus TG8120, Rigaku, Japan). The samples were heated in air from room temperature (RT) to 1300 K at a rate of 20 K/min. X-ray photoelectron spectroscopy (XPS) was performed with an XP spectrometer (PHI-5500MC, ULVAC PHI, Japan) using Mg Kα radiation at 400 W. The diameter of the X-ray beam was 800 μm, the take-off angle was 45°, and the base pressure was below 3×10^{-8} Pa. The charge-up effects were corrected by adjusting the binding energy of C 1s to 284.6 eV. The average oxidation state (AOS) of the samples was measured by titration, as described in a previous report [23]. The amount of the incorporated K (*x* value) in the sample K-OMS-2 was determined by using an inductively coupled plasma with atomic emission spectrometry (ICP-AES; CIROS 120EOP, Rigaku, Japan). The Brunauer–Emmett–Teller (BET) surface area was measured by single-point N_2 adsorption at 77 K, using an automatic surface area analyzer (MS4232-III, MICRO DATA Co., Ltd., Japan) after pretreatment at 473 K for 20 min. Oxygen temperature-programmed desorption (O_2-TPD) was performed in a fixed-bed reactor. In order to remove adsorbed gases, 200 mg of the catalyst was heated in a 20-mL/min He flow at 673 K for 20 min. For O_2 pre-adsorption, the catalyst was heated in a 20-mL/min O_2 flow at 673 K for 20 min and then cooled to room temperature.

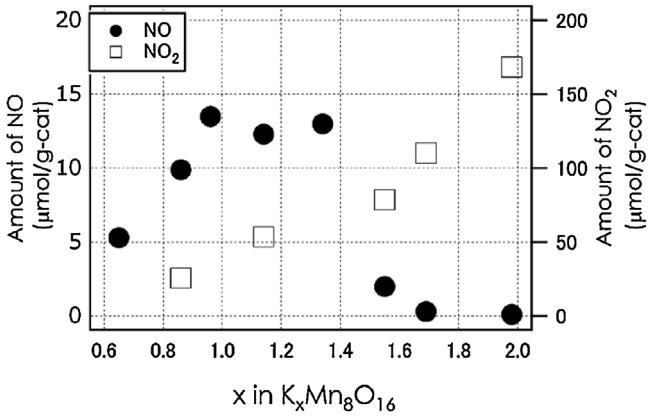

Fig. 1. Effect of K concentration (*x*) on the amount of NO or NO_2 adsorbed at 323 K. Feed gas for NO or NO_2 adsorption: NO or NO_2 (100 ppm), O_2 (10%), CO_2 (10%), CO (800 ppm), C_3H_6 (400 ppm C), and H_2O (5%).

After purging the catalyst with He for 30 min at room temperature, the catalyst was heated to 1073 K at 20 K/min under a 20 mL/min He flow. The corresponding O_2 desorption spectrum was obtained using a quadruple mass spectrometer (Q-MS).

2.3. Performance tests

The performance of every sample as a low-temperature NO_x adsorbent was estimated using a conventional fixed-bed flow reactor (Bex-5900, CATA-5000, Best Instruments Co., Ltd., Japan). The concentrations of NO_x, hydrocarbons, CO, CO_2, and O_2 were measured with a chemiluminescence analyzer, a flame-ionization detector, a nondispersive infrared analyzer, and a paramagnetic analyzer, respectively. The total gas flow rate was held constant at 5.0 L/min, and the concentrations of the various gas components were adjusted using individual mass flow controllers (see Table 2).

To remove pre-adsorbed gases, 1.0 g of the test sample was exposed to a pre-reduction gas at 673 K for 5 min and then to a pre-oxidation gas at 673 K for 5 min. Next, the sample was exposed to the gas mixture containing NO or NO_2 at 323 K for 15 min. The amount of adsorbed NO_x was calculated by measuring the NO_x concentration in the out-flowing gas mixture [6] (Fig. S1).

2.4. Analysis of adsorbed NO_x

The species adsorbed on the surfaces of the K-OMS-2 samples were determined by Fourier-transform infrared (FTIR) spectroscopy. The FTIR spectra were recorded using a Nicolet NEXUS670 system (Thermo Scientific, USA) with a diffuse-reflectance infrared Fourier-transform spectroscopy (DRIFTS) attachment. The test sample was placed in the DRIFTS reactor cell and pretreated in a mixed flow of 10% O_2 in N_2 (200 mL/min) at 673 K for 10 min to remove carbonates and adsorbed gases. Next, the IR spectrum of the sample was recorded after exposure to a mixture of 0.1% NO (or 0.1% NO_2) and 10% O_2 in N_2 at 323 K for 15 min [6].

3. Results and discussion

Fig. 1 shows the amounts of NO and NO_2 adsorbed by $K_xMn_8O_{16}$ at 323 K as functions of the K concentration. The K concentration did not change before and after performance test (Table S1). During these measurements, the samples were exposed to NO in the presence of CO_2 and CO. As mentioned earlier, the NO-adsorption phenomenon is hampered by the presence of other gases. Therefore, the amount of NO adsorbed by $K_{1.14}Mn_8O_{16}$ in the presence of the other gases (12.3 μmol/g) was much smaller than that in

Table 1
Material synthesis conditions. The value of x in $K_xMn_8O_{16}$ was determined by ICP-AES.

Value of x in $K_xMn_8O_{16}$	Molar ratio, $KMnO_4$/Mn(Ac)2·4H_2O	Aging temperature and duration (K, h)		Duration of deionized-water washing cycle	Post-synthesis treatment
0.65	2:3	353	4	3	NH_3
0.86	2:3	353	4	3	HNO_3
0.96	2:3	353	4	5	–
1.14	2:3	353	4	4	–
1.34	2:3	353	4	3	–
1.55	2:3	373	4	3	–
1.69	1:1	353	4	3	–
1.98	3:7	353	4	3	–

Table 2
Components of the gas mixture used to test the NO_x-adsorption performance.

Gas mixture composition	O_2 (%)	CO_2	H_2O	NO (ppm)	NO_2	CO	C_3H_6	H_2
Pre-treatment								
Pre-reduction	0	10	5	0	0	1300	0	900
Pre-oxidation	10	10	5	0	0	0	0	0
NO_x adsorption								
NO adsorption	10	10	5	100	0	800	400	0
NO_2 adsorption	10	10	5	0	100	800	400	0

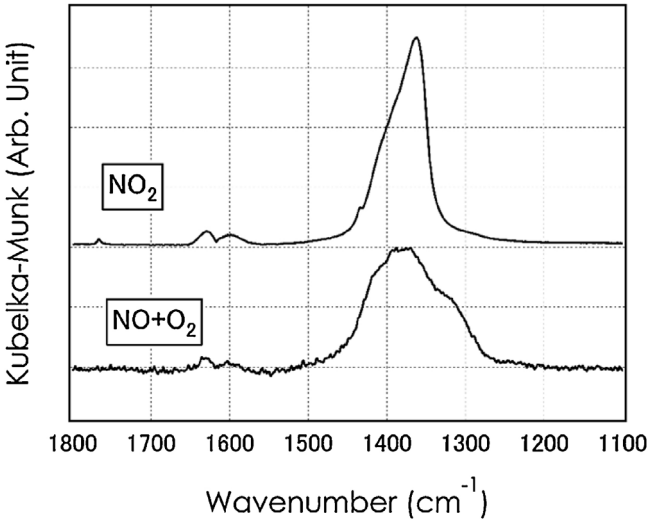

Fig. 2. IR spectra after NO adsorption or NO_2 adsorption at 323 K. Feed gas: NO or NO_2 (0.1%), and O_2 (10%) at 323 K.

the absence of other gases (88.9 μmol/g). In contrast, under the same conditions, NO-adsorbing materials such as Ba/Pt/Al_2O_3 and Ag/Al_2O_3 (Ref. 5) do not adsorb NO. Moreover, the adsorbed NO_x was released by thermal aging between 573 and 773 K, and K-OMS-2 adsorbed NO again at low temperature. The amount of adsorbed NO_2 increased with the increase in K content, indicating that the K sites acted as sites for NO_x adsorption. The $K_xMn_8O_{16}$ samples with $x < 1.5$ adsorbed NO, while the samples with $x > 1.5$ did not, indicating that increasing the K concentration (i.e., the number of NO_x adsorption sites) did not have an impact on the amount of NO adsorbed under these conditions. Since $K_{1.14}Mn_8O_{16}$ showed enough NO adsorption activity, $K_{1.14}Mn_8O_{16}$ was mainly characterized. Fig. 2 shows the FTIR difference spectra of NO and NO_2 adsorbed on the $K_{1.14}Mn_8O_{16}$ sample at 373 K. In all cases, the adsorbed NO_x species were NO_3^- anions [25] at a wavenumber of around ~1380 cm^{-1}, which can be assigned to the stretching band. At wavenumbers above 1800 cm^{-1}, there were no peaks corresponding to adsorbed NO [6]. The presence of this band suggests

Table 3
Characterization results. The specific surface area was measured by single-point N_2 adsorption at 77 K. The crystalite size on the (211) plane was calculated by Scherrer's equation. The average oxidation state (AOS) of the samples was measured by titration.

Value of x in $K_xMn_8O_{16}$	Specific surface area (m^2/g)	(211) crystallite size (nm)	AOS
0.65	77.3	19.7	3.72
0.86	88.7	22.3	3.77
0.96	79.4	23.4	3.71
1.14	82.9	19.6	3.72
1.34	61.7	22.8	–
1.55	71.3	21.4	–
1.69	46.9	33.6	3.77
1.98	33.1	31.5	3.67

that NO oxidized as NO_2 on the $K_xMn_8O_{16}$ and NO_2 is converted into nitrate species. This result also suggests that the K sites worked as adsorption sites of NO_x.

The TEM image of a K-OMS-2 sample ($K_{1.14}Mn_8O_{16}$) in Fig. 3(a) shows that the K-OMS-2 particles had a nanorod-like structure (the other samples also exhibited a similar structure). The average particle length and width of the $K_{1.14}Mn_8O_{16}$ sample were approximately 57 and 15 nm, respectively. Fig. 3(b) shows the cross-sectional structure of the sample. As previously reported, crystal growth occurred along the c-axis [26]. The 2×2 tunnel structure of OMS-2 can be seen at the end of the rod-like particles.

Fig. 4 shows the XRD patterns of the synthesized K-OMS-2 samples with different K content. All the diffraction peaks could be indexed to pure hollandite-type manganese oxide (JCPDS card No. 00-029-1020; tetragonal; space group: $I6/m$). Furthermore, no peaks attributable to other manganese species were observed. The specific surface area (SSA), crystallite size calculated from the XRD patterns ((211) reflection at 37.62°), and AOS values of the K-OMS-2 samples are listed in Table 3. The SSA of the samples decreased from approximately 80 to 30 m^2/g when the x value of $K_xMn_8O_{16}$ was increased from 0.65 to 1.98 owing to crystal growth. The AOS values of the K-OMS-2 samples were almost similar despite the differences in their K content. Since the calculated AOS of $K_2Mn_8O_{16}$ was 3.75, it is assumed that either H^+ or H_3O^+ ions occupied the vacant sites or the oxidation state of potassium changed. Fig. 5(a)

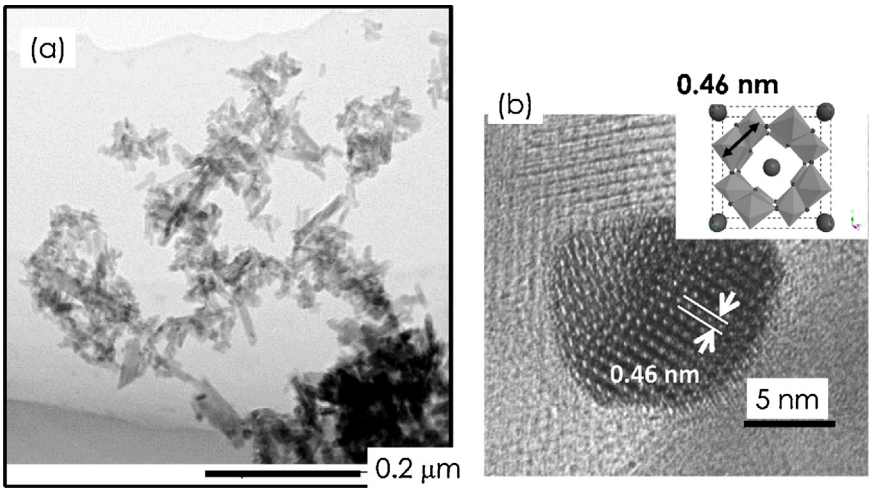

Fig. 3. TEM images of $K_{1.14}Mn_8O_{16}$: (a) overall and (b) cross-sectional views.

and (b) show the Mn 2p and K 2p XPS spectra, respectively, of $K_{1.14}Mn_8O_{16}$, $K_{1.69}Mn_8O_{16}$, and $K_{1.98}Mn_8O_{16}$. The spectra indicate that the oxidation state of manganese was almost the same in all the samples, which agree with the AOS values obtained by titration and X-ray absorption fine structure (XAFS) measurements (Fig. S2). The position of the K $2p_{3/2}$ peak for $K_{1.14}Mn_8O_{16}$ was 292.0 eV. A slight shift of the K $2p_{3/2}$ peak toward higher energy levels was observed for $K_{1.69}Mn_8O_{16}$ (292.3 eV) and $K_{1.98}Mn_8O_{16}$ (292.6 eV). The observed peak shifts in those compounds suggest the formation of metallic-like K—K bonds [27] caused by excess K content in the microporous tunnel structure shown in Fig. 3. From these results, it is considered that the constant AOS of the K-OMS-2 samples with various K content was attained by changing the oxidation state of potassium.

The thermal stabilities of the K-OMS-2 samples in air were determined using TG-DTA. Fig. 6 shows the TG-DTA results for $K_{1.14}Mn_8O_{16}$ in air at temperatures ranging from RT to 1273 K at a ramping rate of 20 K/min. Gradual weight loss was observed between RT and 623 K, between 623 and 873 K, and between 900 and 1100 K. There were also three endothermic peaks and rapid

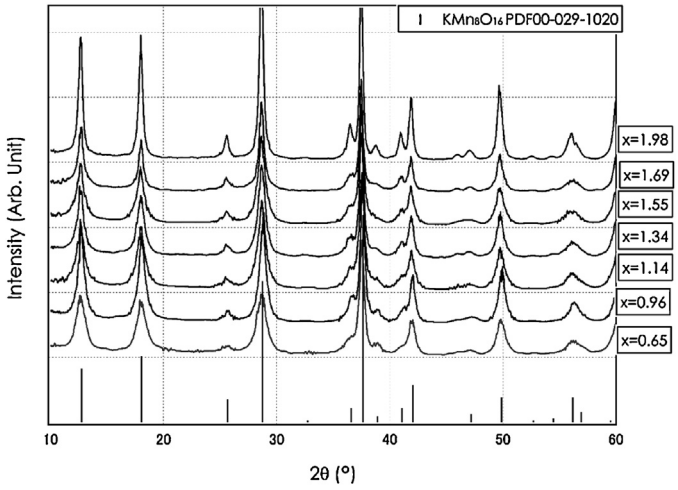

Fig. 4. X-ray diffraction patterns of samples with different K content (x).

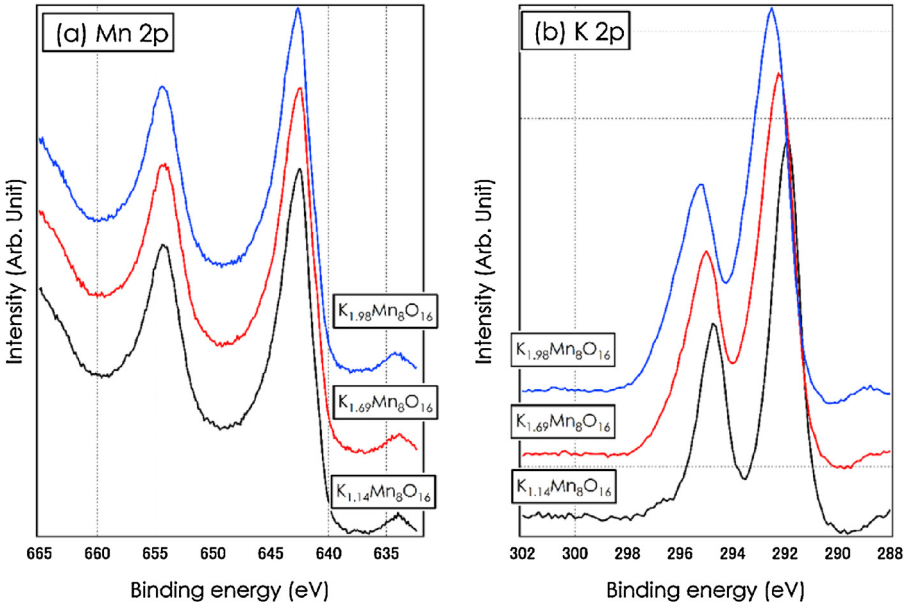

Fig. 5. XPS spectra of the as-prepared K-OMS-2 samples: (a) Mn 2p; (b) K 2p.

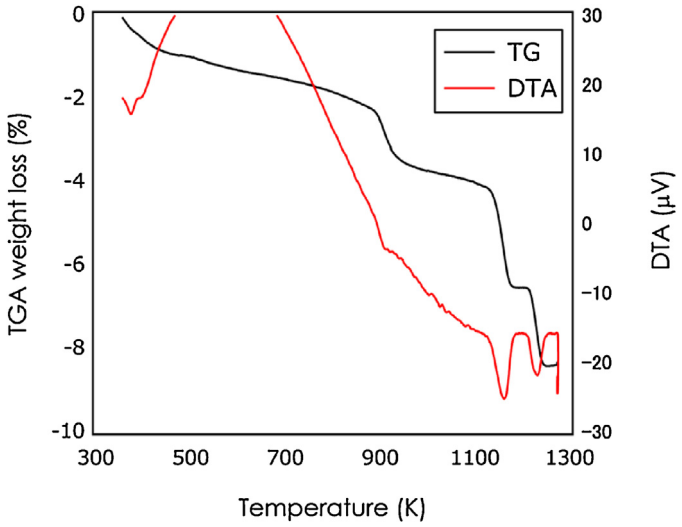

Fig. 6. TG-DTA curve for $K_{1.14}Mn_8O_{16}$ measured in air from RT to 1300 K at a rate of 20 K/min.

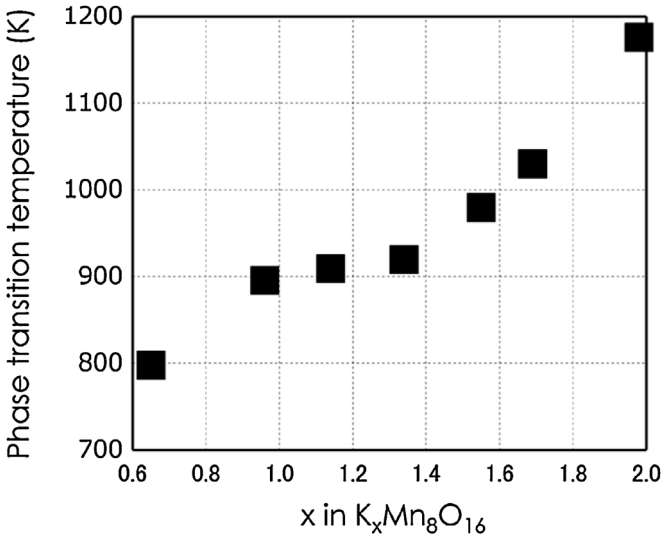

Fig. 7. Phase-transition temperature of K-OMS-2.

weight loss at approximately 905, 1157, and 1224 K. The TG-DTA results, in combination with those of previous reports [12,28,29], indicate that there was a weight loss of 1.5% for $K_{1.14}Mn_8O_{16}$ between RT and 623 K owing to the evolution of H_2O and CO_2. Furthermore, there was a weight loss of 1.1% between 623 and 873 K owing to the evolution of O_2. The endothermic peak at approximately 893 K, which corresponds to a 1.5% weight loss, is attributable to the evolution of O_2 and the phase transition of $K_{1.14}Mn_8O_{16}$ into potassium-occupied $K_2Mn_8O_{16}$ and bixbyite (Mn_2O_3). The endothermic peaks and weight loss around 1130 and 1234 K correspond to the transformation of $K_2Mn_8O_{16}$ to $K_2Mn_4O_8$ and bixbyite to hausmannite, respectively [12,29].

$$K_xMn_8O_{16} \rightarrow K_2Mn_8O_{16} + Mn_2O_3$$

$$(893\,K) \rightarrow K_2Mn_4O_8 + Mn_2O_3$$

$$(1130\,K) \rightarrow K_2Mn_4O_8 + Mn_3O_4 (1234\,K)$$

Fig. 7 shows that the temperature for the phase transition of K-OMS-2 (hollandite-type manganese oxide) into bixbyite increased with increasing K content, suggesting that increasing the K content increased the thermal stability of K-OMS-2 because the lattice

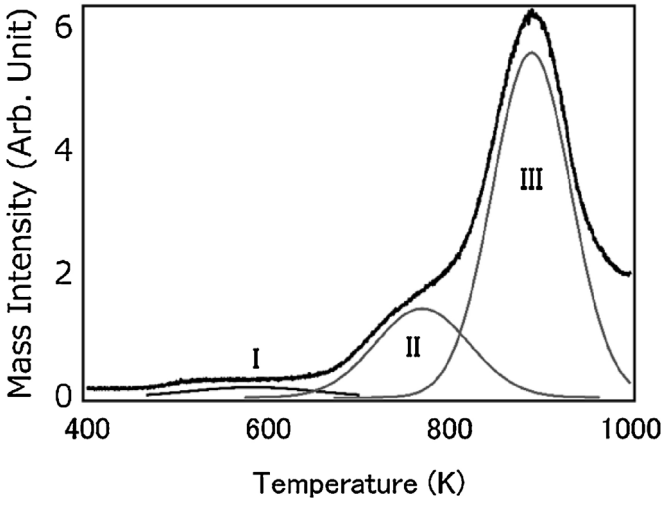

Fig. 8. O_2-desorption properties of $K_{1.14}Mn_8O_{16}$ as it was heated from RT to 1073 K at 20 K/min under a 20-mL/min He flow.

oxygen became more stable. The amounts of O_2 released by these samples, a measure of the degree of NO oxidation, were measured through the temperature-programmed desorption of oxygen (O_2-TPD). Fig. 8 shows the oxygen-releasing properties of $K_{1.14}Mn_8O_{16}$ measured by O_2-TPD. $K_{1.14}Mn_8O_{16}$ started to produce O_2 at 450 K (peak I), releasing a significant amount of O_2 between 650 and 800 K (peak II). Weak adsorption of O on the surface of OMS-2 is considered to be the cause of peak I, and hence, the intensity of peak I from each sample is almost constant. It is evident from the combined TG-DTA and O_2-TPD results that the evolution of O_2 at temperatures above 800 K (peak III) was caused by a phase transition of K-OMS-2 into bixbyite. As described in a previous report [9], the phase-transition temperature of K-OMS-2 in an inert atmosphere is lower than that in air. Therefore, the oxygen indicated by peak II must have been released from the OMS-2 lattice while maintaining its structure and causing the vacancy site to function as an active site.

These results indicate that increasing the K concentration, (i.e., the number of NO_x adsorption sites) did not affect the amount of NO adsorbed under these conditions. A comparison of the SSAs of the K-OMS-2 samples with the amounts of NO adsorbed by them suggested that the amount of adsorbed NO was probably not determined by the SSA value. $K_{0.96}Mn_8O_{16}$ (79.4 m^2/g, 13.5 μmol/g) exhibited better NO-adsorption performance than $K_{1.55}Mn_8O_{16}$ (71.3 m^2/g, 2 μmol/g), even though the two had almost similar SSA values. This suggests that the chemical properties of the K-OMS-2 samples, not their SSA values, were responsible for the differences observed in their adsorption performances. Fig. 9 shows the relationship between the amounts of O_2 released at peak II in a He atmosphere, as well as the amount of NO adsorbed at 323 K. The amount of NO adsorbed at 323 K increased with the increase in the amount of oxygen released, indicating that the oxygen-releasing sites acted as oxidation sites for NO gas at 323 K. In a similar way, the oxygen-releasing sites acted as oxidation sites for CO gas at 575 K (Fig. S3). The amounts of O_2 released at peak II decreased with the increase in the K content. As shown in Fig. 7, the thermal stability of K-OMS-2 increased with the increase in K content. It is considered that the O_2 release for NO oxidation occurred with variation of the Mn oxidation state. K-OMS-2 comprised mixed-valence MnO_2 in which charge imbalance on the octahedral framework due to reduction of Mn^{4+} to Mn^{3+} was compensated by K^+ in the tunnel site [30]. In other words, the variation of the oxidation state of Mn needed the local redox exchange reaction of K with the vacancy site in the tunnel. As shown in Fig. 5, the K—K bonds formed in high-K-

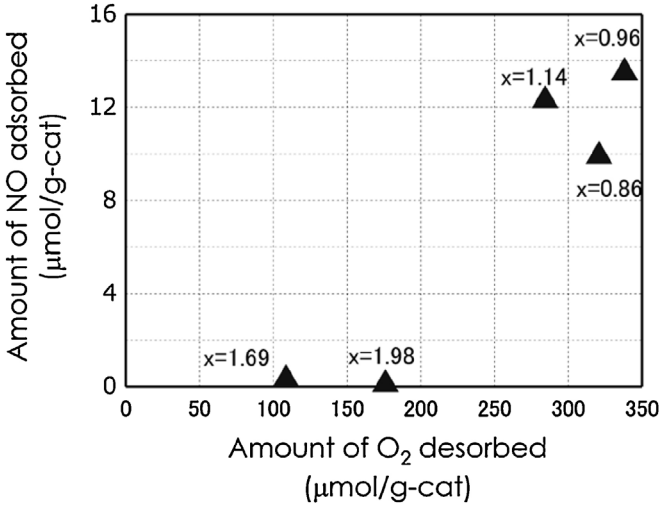

Fig. 9. Relationship between the amount of oxygen released at peak II in a He atmosphere and the amount of NO adsorbed at 323 K. Feed gas for NO adsroption: NO (100 ppm), O_2 (10%), CO_2 (10%), CO (800 ppm), C_3H_6 (400 ppm C), and H_2O (5%).

content K-OMS-2 because the number of vacancy sites in the tunnel site decreased. These results suggest that the increasing K content disturbed the local redox exchange reaction of K with the vacancy site in the tunnel and the variation of the Mn oxidation state, i.e., releasing the lattice oxygen became more difficult. Controlling the K content may alter the oxidation properties of OMS-2, leading to an increase in NO adsorption.

4. Conclusions

K-OMS-2 ($K_xMn_8O_{16}$) samples with different K content were successfully synthesized. The specific surface area of K-OMS-2 decreased with an increase in the K content for $x > 1.5$ owing to crystal growth. The K-OMS-2 samples with $x < 1.5$ exhibited NO adsorption at low temperatures owing to an oxidation reaction. The amount of NO adsorbed depended on the oxidation activity of K-OMS-2 under the test conditions instead of the specific surface area (i.e., the number of NO adsorption sites). At temperatures below 800 K, the amount of adsorbed NO was correlated to the increase in the amount of oxygen released, as estimated by O_2-TPD. It is assumed that the thermally unstable oxygen sites acted as oxidation sites for NO and increased the amount of adsorbed NO.

Appendix A. Supplementary data

Supplementary data associated with this article can be found, in the online version, at http://dx.doi.org/10.1016/j.apcatb.2016.04.023.

References

[1] Y. Tsukamoto, H. Nishioka, D. Imai, Y. Sobue, N. Takagi, T. Tanaka, T. Hamaguchi, Development of new concept catalyst for low CO_2 emission diesel engine using NO_x adsorption at low temperatures, SAE 2012 World Congress & Exhibition (2016), http://dx.doi.org/10.4271/2012-01-0370 (2012-01-0370).
[2] S. Hodjati, K. Vaezzadeh, C. Petit, V. Pitchon, A. Kiennemann, Absorption/desorption of NO_x process on perovskites: performances to remove NO_x from a lean exhaust gas, App. Catal. B Environ. 26 (2000) 5–16.
[3] M. Machida, D. Kurogi, T. Kijima, MnO_x-CeO_2 binary oxides for catalytic NO_x sorption at low temperature selective reduction of sorbed NO_x, Chem. Mater. 12 (2000) 3165–3170.
[4] K. Eguchi, M. Watabe, M. Machida, H. Arai, Selective removal of NO by absorption in mixed oxide catalysts, Catal. Today 27 (1996) 297–305.
[5] S. Tamm, S. Andonova, L. Olsson, Silver as storage compound for NO_x at low temperatures, Catal. Lett. 144 (2014) 674–684.
[6] T. Tanaka, C. Ando, T. Hamaguchi, Y. Ikuta, Improved low temperature removal of NO_x from lean-burn exhaust via adsorption on TiO2-modified Ag–alumina, App. Cataly. A Gen. 464–465 (2013) 296–304.
[7] S.L. Suib, A review of open framework structures, Annu. Rev. Mater. Sci. 26 (1996) 135–151.
[8] K.J. Takeuchi, S.Z. Yau, M.C. Menard, A.C. Marschilok, E.S. Takeuchi, Synthetic control of composition and crystallite size of silver hollandite, $Ag(x)Mn_8O_{16}$: impact on electrochemistry, App. Mater. Interfaces 4 (2012) 5547–5554.
[9] Y. Yin, W. Xu, R. DeGuzman, S.L. Suib, Studies of stability and reactivity of synthetic cryptomelane-like manganese oxide octahedral molecular sieves, Inorg. Chem. 33 (1994) 4384–4389.
[10] X. Chen, Y. Shen, S.L. Suib, C.L. O'Young, Characterization of manganese oxide octahedral molecular sieve (M-OMS-2) materials with different metal cation dopants, Chem. Mater. 14 (2002) 940–948.
[11] R. Kumar, S. Sithambaram, S.L. Suib, Cyclohexane oxidation catalyzed by manganese oxide octahedral molecular sieves—effect of acidity of the catalyst, J. Catal. 262 (2009) 304–313.
[12] Q. Feng, H. Kanoh, Y. Miyai, K. Ooi, Alkali metal ions insertion/extraction reactions with hollandite-type manganese oxide in the aqueous phase, Chem. Mater. 7 (1995) 148–153.
[13] L. Sun, Q. Cao, B. Hu, J. Li, J. Hao, G. Jing, X. Tang, Synthesis, characterization and catalytic activities of vanadium–cryptomelane manganese oxides in low-temperature NO reduction with NH_3, Appl. Catal. A Gen. 393 (2011) 323–330.
[14] H. Zheng, C. Feng, S. Kim, S. Yin, H. Wu, S. Wang, S. Li, Synthesis and electrochemical properties of KMn_8O_{16} nanorods for lithium ion batteries, Electrochem. Acta 88 (2013) 225–230.
[15] H.C. Genuino, M.S. Seraji, Y. Meng, D. Valencia, S.L. Suib, Combined experimental and computational study of CO oxidation promoted by Nb in manganese oxide octahedral molecular sieves, Appl.Catal. B Environ. 163 (2015) 361–369.
[16] O. Sanz, J.J. Delgado, P. Navarro, G. Arzamendi, L.M. Gandia, M. Montes, VOCs combustion catalysed by platinum supported on manganese octahedral molecular sieves, Appl. Catal. B Environ. 110 (2011) 231–237.
[17] F. Schurz, J.M. Bauchert, T. Merker, T. Schleid, H. Hasse, R. Glaser, Octahedral molecular sieves of the type K-OMS-2 with different particle sizes and morphologies: impact on the catalytic properties in the aerobic partial oxidation of benzyl alcohol, Appl. Catal. A Gen. 355 (2009) 42–49.
[18] S. Sithambaram, E.K. Nyutu, S.L. Suib, OMS-2 catalyzed oxidation of tetralin: a comparative study of microwave and conventional heating under open vessel conditions, Appl. Catal. A Gen. 348 (2008) 214–220.
[19] J. Li, R. Wang, J. Hao, Role of lattice oxygen and Lewis acid on ethanol oxidation over OMS-2 catalyst, J. Phys. Chem. C 114 (2010) 10544–10550.
[20] R. Ghosh, X. Shen, J.C. Villegas, Y. Ding, K. Malinger, S.L. Suib, Role of manganese oxide octahedral molecular sieves in styrene epoxidation, J. Phys. Chem. B 110 (2006) 7592–7599.
[21] V.D. Makwana, Y. Son, A.R. Howell, S.L. Suib, The role of lattice oxygen in selective benzyl alcohol oxidation using OMS-2 catalyst: a kinetic and isotope-llabeling study, J. Catal. 210 (2002) 46–52.
[22] L. Espinal, W. Wong-Ng, J.A. Kaduk, A.J. Allen, C.R. Snyder, C. Chiu, D.W. Siderius, L. Li, E. Cockayne, A.E. Espinal, S.L. Suib, Time-dependent CO_2 sorption hysteresis in a one-dimensional microporous octahedral molecular sieve, J,. Am. Chem. Soc. 134 (2012) 7944–7951.
[23] A.R. Gandhe, J.S. Rebello, J.L. Figueiredo, J.B. Fernandes, Manganese oxide OMS-2 as an effective catalyst for total oxidation of ethyl acetate, Appl. Catal. B 72 (2007) 129–135.
[24] Y. Ding, X. Shen, S. Sithambaram, S. Gamez, R. Kumar, V.M.B. Crisostomo, S.L. Suib, M. Aindow, Synthesis and catalytic activity of cryptomelane-type manganese dioxide nanomaterials produced by a novel solvent-free method, Chem. Mater. 17 (2005) 5382–5389.
[25] K.I. Hadjiivanov, Identification of neutral and charged N_xO_y surface species by IR spectroscopy, Catal. Rev. Sci. Eng. 42 (2000) 71–144.
[26] J.C. Villegas, L.J. Garces, S. Gomez, J.P. Durand, S.L. Suib, Particle size control of cryptomelane nanomaterials by use of H_2O_2 in acidic C conditions, Chem. Mater. 17 (2005) 1910–1918.
[27] J.F. Moulder, W.F. Stickle, P.E. Sobol, K.D. Bomben, Handbook of X-ray Photoelectron Spectroscopy, Perkin-Elmer Corp., Eden Prairie, MN, 1992.
[28] J. Luo, Q. Zhang, J. Garcia-Martinez, S.L. Suib, Adsorptive and acidic properties, reversible lattice oxygen evolution, and catalytic mechanism of cryptomelane-type manganese oxides as oxidation catalysts, J. Am. Chem. Soc. 130 (2008) 3198–3207.
[29] R.N. Deguzman, Y. Shen, E.J. Neth, S.L. Suib, C. O'Young, S. Levine, J.M. Newsam, Synthesis and characterization of octahedral M molecular sieves (OMS-2) having the hollandite structure, Chem. Mater. 6 (1994) 815–821.
[30] C. Calvert, R. Joesten, K. Ngala, K. Villegas, A. Morey, X. Shen, S.L. Suib, Synthesis, characterization, and rietveld refinement of tungsten-framework-doped porous manganese oxide (K-OMS-2) material, Chem. Mater. 20 (2008) 6382–6388.